Biosensors and Bioelectronics 82 (2016) 26–31

Contents lists available at ScienceDirect

Biosensors and Bioelectronics

journal homepage: www.elsevier.com/locate/bios

Turn-on near-infrared electrochemiluminescence sensing of thrombin based on resonance energy transfer between CdTe/CdS $core_{small}$/$shell_{thick}$ quantum dots and gold nanorods

Jing Wang [a,b], Xiaochun Jiang [a,c], Heyou Han [a,*]

[a] State Key Laboratory of Agricultural Microbiology, College of Science, Huazhong Agricultural University, Wuhan 430070, PR China
[b] College of Chemical Engineering, Zhejiang University of Technology, Hangzhou 310014, PR China
[c] Hubei Key Laboratory for Processing and Application of Catalytic Materials, College of Chemical Engineering, Huanggang Normal University, Huangzhou 438000, PR China

ARTICLE INFO

Article history:
Received 15 January 2016
Received in revised form
13 March 2016
Accepted 22 March 2016
Available online 24 March 2016

Keywords:
Near-infrared
Electrochemiluminescence resonance energy transfer
CdTe/CdS quantum dots
Gold nanorods
Thrombin
Aptasensor

ABSTRACT

Here we designed a near-infrared electrochemiluminescence (NECL) aptasensor for turn-on ultrasensitive determination of thrombin. It was based on the ECL resonance energy transfer (ECL-RET) of CdTe/CdS $core_{small}$/$shell_{thick}$ quantum dots (QDs) to gold nanorods (AuNRs). AuNRs which functioned as ECL acceptors were assembled onto CdTe/CdS film by DNA hybridization between aptamers and their complementary oligonucleotides. In the absence of thrombin, the NECL of QDs was quenched as a result of the ECL-RET of QDs to AuNRs. In the presence of thrombin, the NECL of the system was "turned on" because thrombin can replace the AuNRs onto the QDs film, owing to the specific aptamer-protein affinity interactions. In this way, the increment of ECL intensity and the concentration of thrombin showed a logarithmic linear correlation in the range of 100 aM to 10 fM with a detection limit of 31 aM (S/N=3). Importantly, the developed aptasensor was successfully applied to thrombin sensing in real serum samples.

1. Introduction

Near-infrared (NIR) fluorescence detection is widely recognized as an effective method for high sensitivity bioapplication benefiting from its attractive merits such as improved tissue penetration, lower background interference, and reduced photochemical damage (Amiot et al., 2008; Ma and Su, 2010). Similarly to NIR fluorescence, NIR electrochemiluminescence (NECL) analysis has emerged as an alternative to traditional visible-range ECL bioassays, especially in some complex biological systems (Wang and Han, 2013). This is because the incorporation of NIR spectral region with ECL technique could minimize the background signal and provide the possibility to fulfill the requirement of interference-free sensing. There have been tremendous efforts to develop high-efficiency ECL emitters for NECL analysis. Semiconductor quantum dots (QDs) hold great promise as a new generation of ECL emitters owing to their size or surface-dependent luminescence and photochemical stability (Ding et al., 2002). While QDs as ECL probes in visible-range have been well developed (Bertoncello and Forster, 2009; Hu and Xu, 2010), NECL from QDs emitters have been much less explored because of their relatively weak and unstable emission signal, as well as low sensitivity captured by the detectors of ECL instruments (Cui et al., 2012; Sun et al., 2008). Furthermore, such rational sensing strategies of traditional visible ECL may be not suitable for NECL detecting in some cases. Only recently, the dual-stabilizer-capped CdTe QDs were synthesized through a convenient one-pot approach (Liang et al., 2011b) and have been used as NECL probes for small molecule and target antigen detection with high sensitivity (Liang et al., 2012; Liang et al., 2011a; Zou et al., 2011). Our group also reported the NECL behaviors from core/shell CdTe/CdS QDs (Wang et al., 2011a) and several NECL biosensors have been constructed in both cathodic and anodic regions (Wang et al., 2012; Wang and Jiang, 2015). Despite these advances, much work is still needed to obtain robust NECL emitters for practical applications.

Luminescence resonance energy transfer (LRET), often occurring between a suitably matched acceptor and donor pair, is an attractive technique for sensitive detection of biomolecules (Sapsford et al., 2006). Various types of LRET including fluorescence resonance energy transfer, chemiluminescence resonance energy transfer and bioluminescence resonance energy transfer have established a sensing platform in the bioapplication (Frigerio et al., 2012). Nowadays, with the progress of ECL technical analysis, ECL resonance energy transfer (ECL-RET) received increasing

* Corresponding author.
E-mail address: hyhan@mail.hzau.edu.cn (H. Han).

http://dx.doi.org/10.1016/j.bios.2016.03.057
0956-5663/

attention in sensing applications of ion, small molecule, protein, and DNA (Wu et al., 2014). Although the current ECL-RET systems were mainly located in the visible range (Lei et al., 2015; Liang et al., 2016; Qi et al., 2013; Shan et al., 2009, 2010; Wang et al., 2016), their sensing strategy could be applicable for NECL biosensors provided that the energy-overlapping donor-acceptor pair is found. Notably, gold nanorods (AuNRs) with distinctive shape-dependent surface plasmon resonance are highly absorbent of light in the NIR region and can act as an acceptor by absorbing the NIR emission (Xu et al., 2011). Inspired by this, a NECL protocol involving ECL-RET from double shelled CdSeTe/CdS/ZnS QDs to AuNRs was reported (Li et al., 2013).

Herein, a turn-on NECL aptasensor for thrombin was developed using an ECL-RET system consisting of CdTe/CdS $core_{small}/shell_{thick}$ QDs and AuNRs. Thrombin is an important physiological protease that plays significant role in many life processes, such as blood solidification, wound cicatrization, and inflammation (Hwang et al. 2001). Therefore, quantitative detection of thrombin at low concentrations is extremely important in clinical diagnosis. The CdTe/CdS QDs film at the glassy carbon electrode (GCE) surface showed a strong and stable NECL emission of 707 nm at *ca.* − 1.45 V. After immobilization with capturing DNA (cDNA, the aptamer of thrombin) and sequential hybridization with probing DNA-modified AuNRs (pDNA-AuNRs), the NECL signal was tremendously quenched through ECL-RET. The spectrum- and distance- dependent quenching efficiency of ECL-RET was studied. After adding thrombin in the system, thrombin G-quadruplex conformation could be formed, and this will dehybridize the double-stranded DNA to release the pDNA-AuNRs from electrode surface. Thus the cathodic NECL of the QDs was recovered. On the basis of concentration-dependent ECL recovery, aptamer-mediated "turn-on" mode combination with the low-interference NIR optical window, this approach exhibited good performance in the detection of thrombin at ultralow concentration. Furthermore, the applicability of the proposed NECL aptasensor in human serum was explored.

2. Material and methods

2.1. Apparatus

The ECL emissions and spectra were performed using a Model MPI-EII ECL Analyzer Systems, and the details on manipulation could be found in previous report (Wang et al. 2012). Data of absorption spectra, photoluminescence (PL) spectra, transmission electron microscopy (TEM), hydrodynamic diameters and zeta potentials were acquired according to the reported method (see details in Supplementary Data, SD).

2.2. Reagents

Thrombin (freeze-dry powder), mercaptopropionic acid (MPA), bovine serum albumin (BSA), tris(2-carboxyethyl)phosphine hydrochloride solution (TCEP), cetyltrimethylammonium bromide (CTAB), and sodium dodecyl sulfate (SDS) were obtained from Sigma-Aldrich Chemical Co. Tellurium powder, cadmium chloride ($CdCl_2 \cdot 2.5H_2O$), sodium borohydride ($NaBH_4$), chloroauric acid ($HAuCl_4 \cdot 3H_2O$), chitosan (> 85% deacetylation), glutaraldehyde (25% aqueous solution), ascorbic acid (AA) and silver nitrate ($AgNO_3$) were purchased from Sinopharm Chemistry Reagent Co., Ltd (Shanghai, China). All other common solvents and salts were of analytical grade and all solutions were prepared with ultrapure water obtained from a Millipore water purification system (≥ 18 MΩ-cm, Milli-Q, Millipore).

All the oligonucleotides were purchased from Shenggong Bioengineering Ltd Company. The sequences of these oligonucleotides employed were given in SD.

2.3. Preparation

The CdTe/CdS $core_{small}/shell_{thick}$ QDs, the CTAB-stabilized AuNRs, and pDNA-AuNRs were synthesized according to previously published procedure with small modifications (see details in SD).

2.4. Fabrication of the NECL aptasensor

First, the bare GCE was polished in sequential order with 1.0, 0.3, and 0.05 μm alumina slurry to obtain a mirror-like surface, followed by sonication in the ultrapure water and ethanol in turn, and finally, dried in air. Next, 6 μL of the prepared QDs solution (1 mg/mL) was cast onto the bare GCE surface and evaporated in air to form a homogeneous film. Because of the abundant active sites (such as –OH, –C=O, and –COOH) on the fresh surface of pretreated GCE, the CdTe/CdS QDs could adsorb on it firmly. Subsequently, to increase the reproducibility of the modified electrode, 3 μL of 0.05% chitosan (Ch) solution was dropped on the above modified electrode (GCE/QD) to produce a smoother and more uniform surface microenvironment for DNA immobilization. After rinsing thoroughly with ultrapure water, the modified electrode (GCE/QD/Ch) was incubated with 5 μL of 2.5% glutaraldehyde solution for 2 h at room temperature to activate the amino groups. After rinsing with 0.1 M Tris–HCl buffer (pH 7.4), the resulting electrode was soaked in 50 μL of 1 μM cDNA solution at 4 °C for at least 12 h. Afterward, 50 μL of 2 wt% BSA was dropped on the electrode (GCE/QD/Ch/cDNA) at 4 °C for 2 h to block the non-specific binding sites. The resultant modified electrode (GCE/QD/Ch/cDNA,BSA) was incubated with 50 μL of pDNA-AuNRs dispersion at 37 °C for 2 h. The obtained modified electrode was thoroughly cleaned with ultrapure water and Tris–HCl buffer to remove the physically absorbed species. The finished aptasensor (GCE/QD/Ch/cDNA,BSA, pDNA-AuNRs) was stored in the refrigerator at 4 °C for further use.

2.5. ECL detection of thrombin

The ECL responses of the proposed aptasensors were investigated in 3 mL of 0.1 M phosphate buffered saline (PBS, pH=7.4) containing 0.1 M $K_2S_2O_8$ and 0.1 M KCl, which are incubated with different concentrations of thrombin solution for 1 h at 37 °C. The working potential was from 0 to − 1.5 V (vs Ag/AgCl) at a scan rate of 200 mV/s, and the voltage of the photomultiplier tube (PMT, R8630) was at 900 V. ECL signals related to the thrombin concentrations could be measured. The schematic graph of the fabrication process of aptamer based assay for thrombin was illustrated in Scheme 1.

3. Results and discussion

3.1. Preparation and Characterization of CdTe/CdS $core_{small}/shell_{thick}$ QDs and AuNRs

MPA-capped CdTe/CdS $core_{small}/shell_{thick}$ QDs with a NIR emission peak at 702 nm (Fig. 1A, curve a) were synthesized on the basis of a previous method (Deng et al., 2010). As a characteristic of type-II QDs (produced by lattice-mismatch strain tuning), the distinctive peak of absorption spectra was unconspicuous after the thick shell coating (Fig. 1A, curve b) (Smith et al., 2008). Representative TEM image (Fig. 1B) shows that the obtained CdTe/CdS $core_{small}/shell_{thick}$ QDs were nearly monodispersed with an average size of 4.6 ± 0.5 nm. The AuNRs, synthesized in the

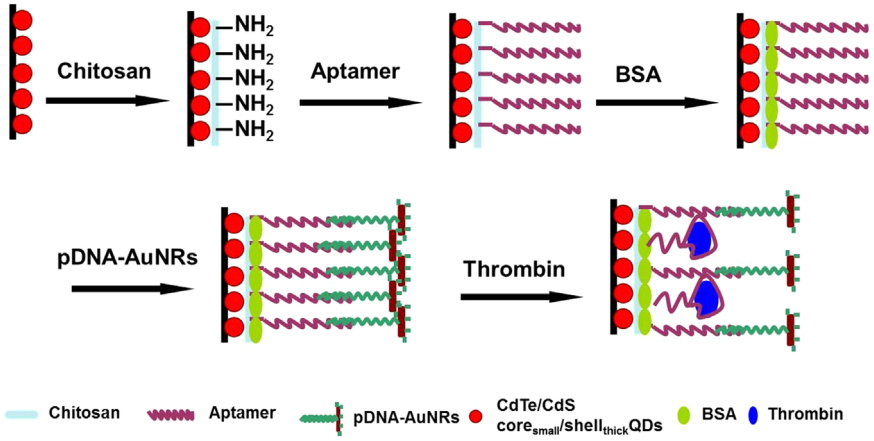

Scheme 1. Schematic illustration of an aptamer-based NECL assay for thrombin.

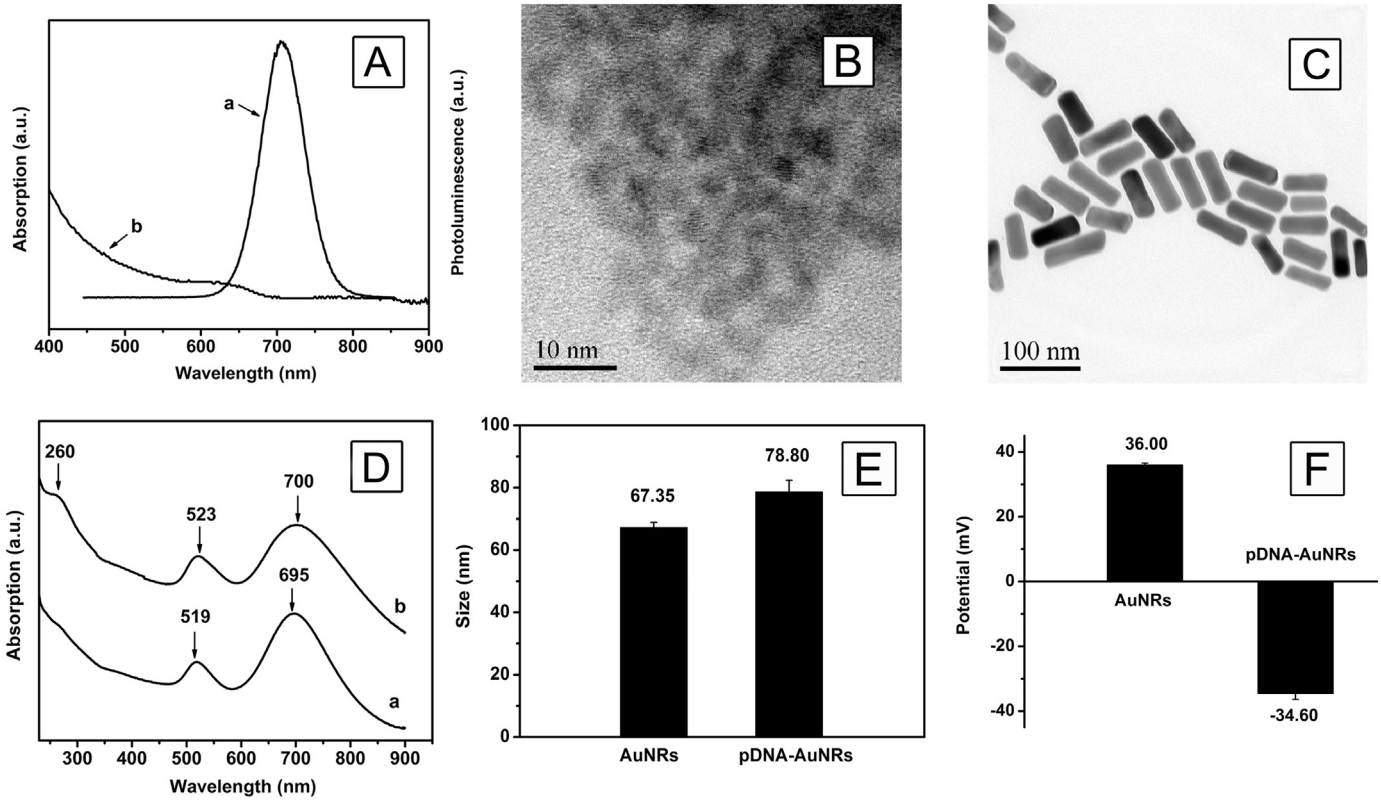

Fig. 1. (A) PL (a) and UV–Vis absorption (b) spectra, and (B) TEM photograph of CdTe/CdS core$_{small}$/shell$_{thick}$ QDs (0.1 mg/mL aqueous solution, λ_{ex}=380 nm). (C) TEM image of AuNRs. (D) UV–Vis absorption spectra of AuNRs before (a) and after (b) linked with pDNA (1 nM AuNRs in 0.01 M CTAB, 1 nM pDNA-AuNRs in 0.01 M Tris–HCl solution, pH 7.4). (E) Size distribution and (F) zeta potential of AuNRs before and after linked with pDNA.

present study by employing a seed-mediated protocol (Nikoobakht and El-Sayed, 2003), exhibit two surface plasma resonance (SPR) bands. One is the transverse band (~520 nm), and the other is the longitudinal band, which can be tuned from 600 to 1300 nm with their aspect ratio (Murphy et al., 2010). According to the TEM observation (Fig. 1C), highly monodispersed AuNRs had an aspect ratio of ~3 with an average diameter of 20 ± 1.5 nm and average length of ~59.5 ± 6.5 nm. They exhibited a longitudinal plasmonic band at ~695 nm and a transverse plasmonic band at ~519 nm (Fig. 1D, curve a). The presence of pDNA on the surface of AuNRs was confirmed by the UV–vis measurements. It could be seen that there was a red shift in both transverse and longitudinal absorption peaks of AuNRs after conjugation with pDNA (Fig. 1D, curve b). This fact may be owing to the change in the refractive index of the medium upon the binding pDNA with AuNRs. Meanwhile, it is reasonable to mention that a slight broadening in both the peaks has taken place due to the increase in size of conjugates (Parab et al., 2010). In addition, a characteristic absorption peak at *ca.* 260 nm in pDNA-AuNRs sample clearly indicated the presence of DNA on the AuNRs surface (Pal et al., 2011). To further identify the coupling, the longitudinal hydrodynamic diameters and zeta potentials of the AuNRs before and after treatment with pDNA were measured. As presented in Fig. 1E, the average longitudinal hydrodynamic diameters of AuNRs in aqueous solution were 67.35 ± 1.5 nm, and pDNA-AuNRs were 78.80 ± 3.6 nm, slightly larger than the AuNRs. The zeta potential of the CTAB-capped AuNRs was positive (+36.00 ± 0.5 mV) but was negative (−34.60 ± 1.8 mV) for pDNA-AuNRs (Fig. 1F). All the results

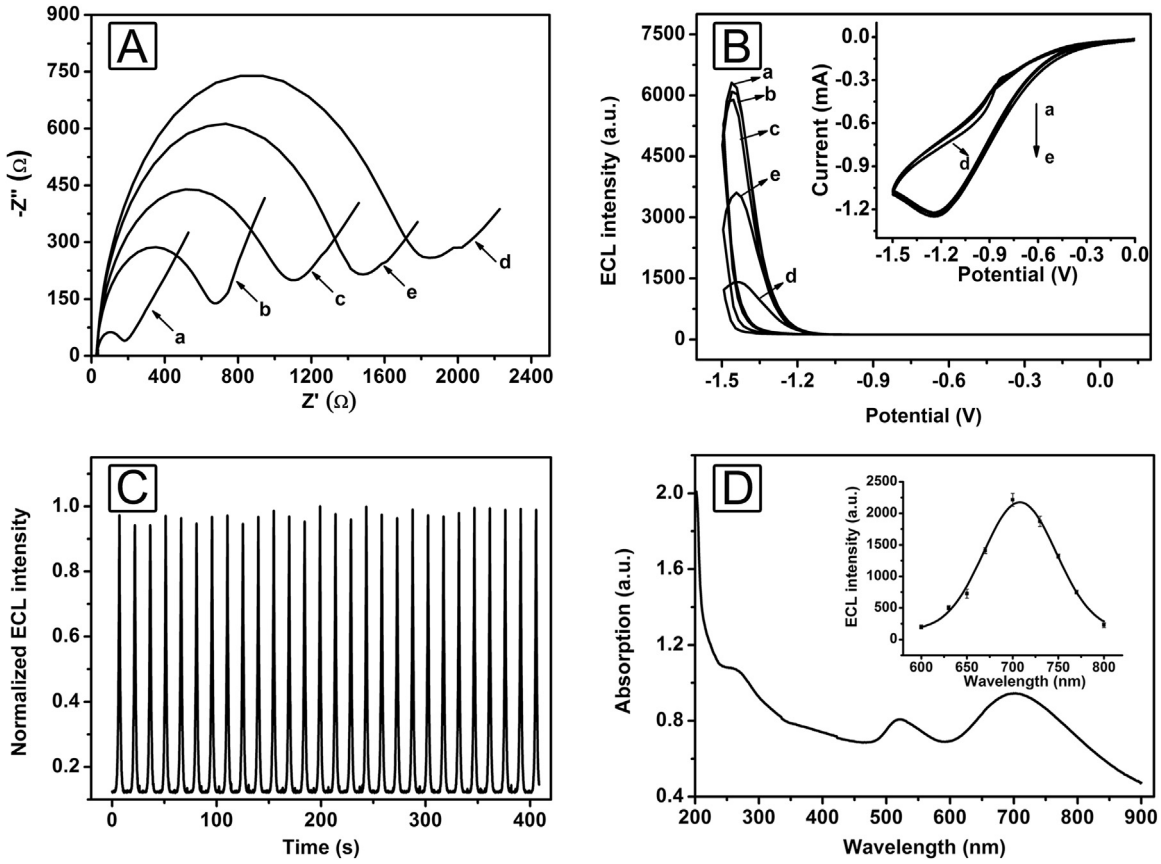

Fig. 2. (A) EIS of bare GCE (a), GCE/QD/Ch (b), GCE/QD/Ch/cDNA (c), GCE/QD/Ch/cDNA,BSA (d), and GCE/QD/Ch/cDNA,BSA,pDNA-AuNRs (e) in 0.10 M KNO_3 containing 0.02 M $K_3[Fe(CN)_6]/K_4[Fe(CN)_6]$. (B) ECL–potential curves of the electrode at different stages in 0.1 M $K_2S_2O_8$ (pH = 7.4) and cyclic voltammograms (CVs, inset) responses of the electrode at different stages in PBS buffer (pH = 7.4) containing 5.0 mM $[Fe(CN)_6]^{3-/4-}$ as redox probe: (a) GCE/QD/Ch, (b) GCE/QD/Ch/cDNA,BSA, (c) GCE/QD/Ch/cDNA, BSA,pDNA, (d) GCE/QD/Ch/cDNA,BSA,pDNA-AuNRs, and (e) GCE/QD/Ch/cDNA,BSA,pDNA-AuNRs incubation with 1 fM thrombin. (C) ECL emission from GCE/QD/Ch/cDNA, BSA,pDNA-AuNRs incubation with 1 fM thrombin under continuous CVs for 30 cycles. (D) UV–Vis absorption spectra of pDNA-AuNRs-700, inset: ECL spectrum of GCE/QD/Ch.

demonstrated that the surface of AuNRs was successfully covered with a certain amount of pDNA. For control experiments, AuNRs with other two different aspect ratios were synthesized by tuning the amounts of added Ag^+, which were characterized by TEM and UV−Vis spectra (Fig. S1). Because of the longitudinal SPR peak values, they were referred to as AuNRs-659 and AuNRs-757, respectively.

3.2. Fabrication and characterization of the NECL-RET aptasensor

As illustrated in Scheme 1, for the fabrication of the NECL aptasensor, the CdTe/CdS QDs QDs were firstly deposited onto the GCE and incubated with chitosan for cDNA (aptamer) immobilization, followed by blocking with BSA. Then, pDNA-AuNRs were brought onto the electrode surface through the hybridization. The stepwise construction process of the aptasensor was characterized by electrochemical impedance spectroscopy (EIS) analysis as shown in Fig. 2A. It was observed that the bare GCE revealed a very small semicircular domain (curve a). After the QDs and chitosan were immobilized onto the electrode, the electron-transfer resistance (R_{et}) just increased somewhat in comparison with bare GCE (curve b). Subsequently, the immobilization of cDNA (curve c) and BSA (curve d) resulted in the great increase of R_{et} value due to their insulating properties (Jie et al., 2008). However, obviously decreased R_{et} could be observed after the pDNA-AuNRs bioconjugates were assembled onto the electrode (curve e), originating from the excellent conductivity of AuNRs (Li et al., 2013). These results were consistent with the fact that the electrode was fabricated as expected.

In order to confirm the feasibility of the method, ECL−potential responses were investigated stepwise, and the results are presented in Fig. 2B. The QDs-modified electrode produced an intensive cathodic ECL emission peak at *ca.* −1.45 V in air-saturated pH 7.4 PBS buffer with $K_2S_2O_8$ as coreactant (curve a). The corresponding ECL processes are listed are as follows:

$$QDs + ne \rightarrow nQDs^{\bullet -} \quad (1)$$

$$S_2O_8^{2-} + e^- \rightarrow SO_4^{2-} + SO_4^{\bullet -} \quad (2)$$

$$QDs^{\bullet -} + SO_4^{\bullet -} \rightarrow QDs^* + SO_4^{2-} \quad (3)$$

$$QDs^* \rightarrow QDs + h\gamma \quad (4)$$

After immobilizing with the cDNA and BSA consecutively, the ECL intensity slightly decreased (curve b) as a result of the increased impedance and inhibition of $S_2O_8^{2-}$ diffusion to the electrode surface. However, after hybridizing with pDNA-AuNRs, the resultant modified electrode exhibited a significant 76.8% decrease in the cathodic ECL intensity (curve d), whereas no obvious ECL decrease appeared from GCE/QDs/Ch/cDNA,BSA,pDNA (curve c) at the same pDNA concentration. Importantly, we observed that there was very small fluctuation in reduction peak current of coreactant and QDs, indicating the big ECL quenching efficiency was not caused by interaction of the assembled pDNA-AuNRs nanocomposites with the coreactant (inset in Fig. 2B) (Shan et al. 2011). Sequentially, after adding 1 fM thrombin, the cathodic ECL signal recovered to 59.1% of GCE/QD/Ch/cDNA,BSA (curve e), which may be ascribed to the

inhibition of ECL-RET between QDs and AuNRs. The increase extent is relative to the amount of thrombin, thus thrombin can be quantitatively detected. Besides, the ECL intensities of the aptasensor after dipping in 1fM thrombin solution for 2 h remained at a comparatively stable value (5.7% variation) during consecutive cyclic potential scanning (Fig. 2C), indicating an acceptable stability for ECL detection.

To demonstrate the quenching mechanism between QDs and AuNRs, the UV – Vis absorption spectrum of pDNA-AuNRs and ECL emission spectrum of GCE/QD/Ch were obtained, respectively (Fig. 2D). The ECL spectrum of the QDs film demonstrated a maximum wavelength of around 707 nm, which significantly overlaps with the absorption spectrum of pDNA-AuNRs, indicating the potential of ECL-RET from the excited QDs to AuNRs.

3.3. Influencing factors on the ECL-RET efficiency

Obviously, enhancement of ECL-RET efficiency is the key to improve the detection sensitivity of the ECL-RET biosensor. The degree of spectral overlap on the ECL-RET efficiency was firstly investigated. Herein, we used the pDNA-AuNRs with longitudinal SPR bands at 661 and 763 nm as the acceptor for parallel experiments (Fig. S1). As displayed in Fig. S2, while pDNA-AuNRs-700 could result in NECL quenching efficiency of 76.8% compared to GCE/QD/Ch/cDNA,BSA (Fig. 2B, curve e), the pDNA-AuNRs-661 and pDNA-AuNRs-763 could just lead to NECL quenching efficiency of 56.0% and 48.1%, respectively. The results proved that the spectrum overlap between donor and acceptor was of great importance and the greater the spectrum overlap will produce higher ECL-RET efficiency. The distance between energy donor and acceptor is also important for the efficiency of energy transfer. By varying the DNA lengths (see details in SD), the separation distance between QDs film and AuNRs can be systematically varied. In this case, AuNRs and the QDs film was separated by chitosan layer (~2 nm) and 15 complementary bases (1 nm for 3-base) (Wang et al., 2011b), the separation distance was about 7 nm after hybridization. Under the same experimental condition, the separation distance of two other control experiments was about 12 and 17 nm by using longer aptamer 2 and aptamer 3 with their complementary pDNAs, respectively. As displayed in Fig. S3, for pDNA-AuNRs-700, the separation distance being about 7 nm exhibited the largest NECL quenching efficiency of 76.8%, while the separation distance of 12 and 17 nm only caused a 51.4% and 45.4% drop, respectively. As a consequence, the aptamer with 15 bases was chosen for further use. Moreover, the effect of hybridization time on quenching efficiency was performed. With the increase in hybridization time, the NECL quenching efficiency greatly enhanced and then reached a plateau at 2 hours (Fig. S4). Therefore, 2 h was recommended for cDNA-pDNA hybridization.

3.4. Thrombin detection with the NECL aptasensor

Taking advantages of the NIR window and highly-efficient ECL-RET, a signal-on NECL biosensing platform was constructed for the detection of thrombin. As demonstrated above, after the thrombin was introduced onto the electrode, the ECL intensity dramatically increases due to the target-induced removal of the pDNA-AuNRs quencher. Fig. 3 illustrates the ECL responses of the aptasensor toward different concentrations of thrombin and the corresponding standard calibration curve for thrombin detection. As a result, a linear relationship between the logarithmic value of thrombin concentration and the ECL intensity increment ($\Delta I = I - I_0$) was plotted in the concentration range of 100 aM to 10 fM. The regression equation was $\Delta I = 1399.13 \log c - 2819.27$ with a correlation coefficient of 0.978, c was the value of thrombin concentration (aM). Meanwhile, the limit of detection (LOD) was estimated to be 31 aM at signal-to-noise ratio S/N=3 without any signal

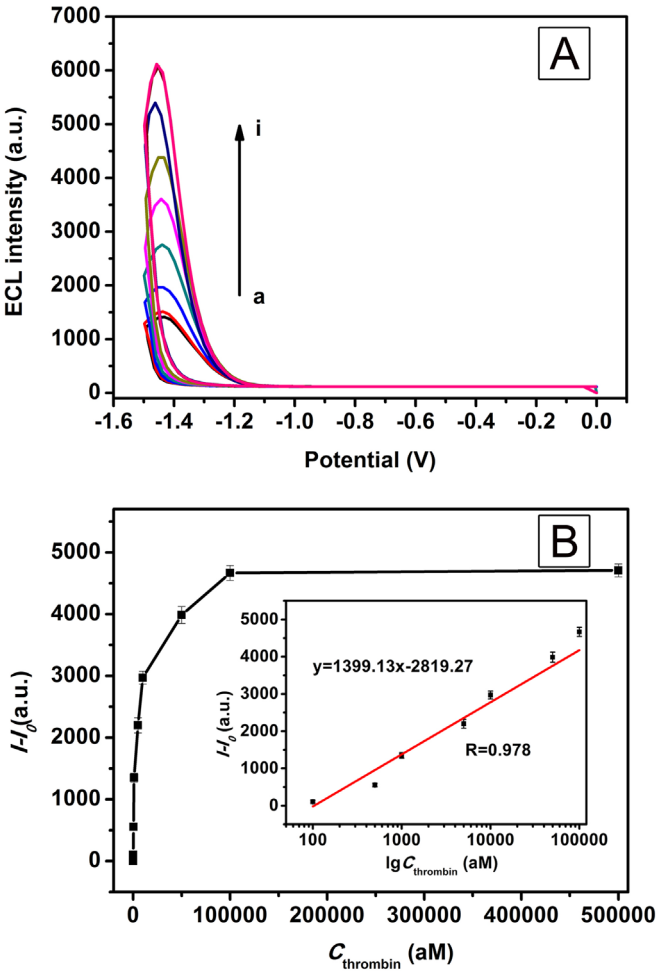

Fig. 3. (A) ECL profiles of the proposed NECL aptasensor in solutions with different concentrations of thrombin (aM) (a) 0, (b) 100, (c) 200, (d) 500, (e) 1000, (f) 2000, (g) 5000, (h) 10,000, (i) 50,000 in 0.1 M pH 7.4 PBS containing 0.1 M $K_2S_2O_8$ and 0.1 M KCl, scanning from 0 V to − 1.5 V with a scan rate of 200 mV/s. (D) Calibration curve for thrombin determination.

amplification events. A comparison between the proposed NECL aptasensor and other ECL aptasensor in the visible range for thrombin is listed in Table S1. It can be seen that the sensitivity of the fabricated NECL aptasensor is superior to most previously reported detection methods for thrombin. The high sensitivity of the aptasensor seems to arise from the low background interference in NIR region, the high ECL-RET efficiency, and smart binding of thrombin and aptamer with turn-on mode.

3.5. Specificity, reproducibility, and stability of the NECL aptasensor

To evaluate the selectivity of the present sensing system, the effects of three proteins of excess concentrations on the ECL intensity of the aptasensor were examined. As shown in Fig. S5, BSA molecules caused a small decrease of the signal, while other proteins (HIgG and Hb) lead to a slight increment of ECL intensity. In contrast to the incubation of the aptasensor with thrombin, the large ECL intensity increment was observed. In particular, a mixed sample did not exhibit major signal change compared with that of thrombin alone. These results indicate that the aptasensor was highly selective due to the good recognition of the aptamer of thrombin and the slight NECL recovery from other proteins may be originated from the nonspecific binding and the larger distance between donor and acceptor (Stobiecka, 2014; Stobiecka and Chalupa, 2015). Reproducibility of the aptasensor for thrombin was

Table 1
Determination of thrombin content in three human serum samples using the proposed NECL aptasensor.

Sample	Added thrombin concentration (fM)	Found thrombin concentration (fM)	Recovery	RSD (n=5)
1	0.5	0.563	112.6%	5.8%
2	1.0	1.083	108.3%	3.3%
3	5.0	5.145	102.9%	3.9%

investigated with intra- and inter-assay precision, which were evaluated by measuring the same thrombin sample with five replicate measurements, and with five aptasensors made on the same electrode. The intra- and inter-assay variation coefficients obtained from 1 fM thrombin were 3.9% and 7.1% respectively, indicating the aptasensor possessed acceptable reproducibility. No obvious change in the ECL intensity was observed after storage in 0.01 M PBS at 4 °C for one month, indicating the good stability of the aptasensor.

The potential applicability of the NECL aptasensor was investigated by determining spiked thrombin in human serum. Before the determination, the samples were prepared by adding thrombin with different concentrations to human serum (provided by Affiliated Hospital, Huazhong Agricultural University). Table 1 describes the results of three independent serum samples obtained using the proposed aptasensor. It was clearly observed that the recoveries and relative standard deviations were in the range of 102.9–112.6% and 3.3–5.8% respectively, which was satisfactory for quantitative assays performed in real biological samples.

4. Conclusion

Taken together, this work has demonstrated a novel ECL-RET system between NIR-emitting CdTe/CdS $core_{small}/shell_{thick}$ QDs as the ECL donors and AuNRs as the ECL acceptors, as well as the fabrication of turn-on aptasensor for ultrasensitive thrombin detection. The highly effective ECL-RET could be attributed not only to their appropriate separation distance but also to their overlapping emission/absorption spectra. By taking advantages of highly effective ECL-RET, smart recognition of aptamer and target protein, and the low background noise of "NIR optical window", the concentration detection limit of 31 aM for thrombin was achieved without any signal amplification events. The potency of this aptasensors has been demonstrated by its successful applications in serum samples. We expect that this NECL aptasensor could pave the way for developing new diagnosis probes for direct detection of biomolecules at very low concentrations without sample pretreatment.

Acknowledgment

We gratefully acknowledge the financial support from National Natural Science Foundation of China (Grant nos. 21375043 and 21405139).

Appendix A. Supplementary material

Supplementary data associated with this article can be found in the online version at http://dx.doi.org/10.1016/j.bios.2016.03.057.

References

Amiot, C.L., Xu, S., Liang, S., Pan, L., Zhao, J.X., 2008. Sensors 8, 3082–3105.
Bertoncello, P., Forster, R.J., 2009. Biosens. Bioelectron. 24, 3191–3200.
Cui, R., Gu, Y.-P., Bao, L., Zhao, J.-Y., Qi, B.-P., Zhang, Z.-L., Xie, Z.-X., Pang, D.-W., 2012. Anal. Chem. 84, 8932–8935.
Deng, Z., Schulz, O., Lin, S., Ding, B., Liu, X., Wei, X., Ros, R., Yan, H., Liu, Y., 2010. J. Am. Chem. Soc. 132, 5592–5593.
Ding, Z., Quinn, B.M., Haram, S.K., Pell, L.E., Korgel, B.A., Bard, A.J., 2002. Science 296, 1293–1297.
Frigerio, C., Ribeiro, D.S.M., Rodrigues, S.S.M., Abreu, V.L.R.G., Barbosa, J.A.C., Prior, J. A.V., Marques, K.L., Santos, J.L.M., 2012. Anal. Chim. Acta 735, 9–22.
Hu, L., Xu, G., 2010. Chem. Soc. Rev. 39, 3275–3304.
Hwang, K.-K., Grossman, J.M., Visvanathan, S., Chukwuocha, R.U., Woods, V.L., Le, D. T., Hahn, B.H., Chen, P.P., 2001. J. Immunol. 167, 7192–7198.
Jie, G., Zhang, J., Wang, D., Cheng, C., Chen, H.-Y., Zhu, J.-J., 2008. Anal. Chem. 80, 4033–4039.
Lei, Y.-M., Huang, W.-X., Zhao, M., Chai, Y.-Q., Yuan, R., Zhuo, Y., 2015. Anal. Chem. 87, 7787–7794.
Li, L., Chen, Y., Lu, Q., Ji, J., Shen, Y., Xu, M., Fei, R., Yang, G., Zhang, K., Zhang, J.R., Zhu, J.J., 2013. Sci. Rep. 3, 1529–1538.
Liang, G., Liu, S., Zou, G., Zhang, X., 2012. Anal. Chem. 84, 10645–10649.
Liang, G., Shen, L., Zou, G., Zhang, X., 2011a. Chem. -Eur. J. 17, 10213–10215.
Liang, G.D., Shen, L.P., Zhang, X.L., Zou, G.Z., 2011b. Eur. J. Inorg. Chem. 25, 3726–3730.
Liang, R.-P., Qiu, W.-B., Zhao, H.-F., Xiang, C.-Y., Qiu, J.-D., 2016. Anal. Chim. Acta 904, 58–64.
Ma, Q., Su, X., 2010. Analyst 135, 1867–1877.
Murphy, C.J., Thompson, L.B., Alkilany, A.M., Sisco, P.N., Boulos, S.P., Sivapalan, S.T., Yang, J.A., Chernak, D.J., Huang, J., 2010. J. Phys. Chem. Lett. 1, 2867–2875.
Nikoobakht, B., El-Sayed, M.A., 2003. Chem. Mater. 15, 1957–1962.
Pal, S., Deng, Z., Wang, H., Zou, S., Liu, Y., Yan, H., 2011. J. Am. Chem. Soc. 133, 17606–17609.
Parab, H.J., Jung, C., Lee, J.-H., Park, H.G., 2010. Biosens. Bioelectron. 26, 667–673.
Qi, W., Wu, D., Zhao, J., Liu, Z., Zhang, W., Zhang, L., Xu, G., 2013. Anal. Chem. 85, 3207–3212.
Sapsford, K.E., Berti, L., Medintz, I.L., 2006. Angew. Chem. Int. Ed. 45, 4562–4589.
Shan, Y., Xu, J.-J., Chen, H.-Y., 2009. Chem. Commun. 45, 905–907.
Shan, Y., Xu, J.-J., Chen, H.-Y., 2010. Chem. Commun. 46, 5079–5081.
Shan, Y., Xu, J.-J., Chen, H.-Y., 2011. Nanoscale 3, 2916–2923.
Smith, A.M., Mohs, A.M., Nie, S., 2008. Nat. Nanotechnol. 4, 56–63.
Stobiecka, M., 2014. Biosens. Bioelectron. 55, 379–385.
Stobiecka, M., Chalupa, A., 2015. J. Phys. Chem. B 119, 13227–13235.
Sun, L., Bao, L., Hyun, B.-R., Bartnik, A.C., Zhong, Y.-W., Reed, J.C., Pang, D.-W., Abruña, H.c.D., Malliaras, G.G., Wise, F.W., 2008. Nano Lett. 9, 789–793.
Wang, J., Han, H., 2013. Rev. Anal. Chem. 32, 91–101.
Wang, J., Han, H., Jiang, X., Huang, L., Chen, L., Li, N., 2012. Anal. Chem. 84, 4893–4899.
Wang, J., Jiang, X., 2015. Sens. Actuat. B-Chem. 207 Part A, 552–555.
Wang, J., Jiang, X., Han, H., Li, N., 2011a. Electrochem. Commun. 13, 359–362.
Wang, J., Shan, Y., Zhao, W.-W., Xu, J.-J., Chen, H.-Y., 2011b. Anal. Chem. 83 (11), 4004–4011.
Wang, Q., Chen, M., Zhang, H., Wen, W., Zhang, X., Wang, S., 2016. Biosens. Bioelectron. 79, 561–567.
Wu, P., Hou, X., Xu, J.-J., Chen, H.-Y., 2014. Chem. Rev. 114, 11027–11059.
Xu, L., Kuang, H., Wang, L., Xu, C., 2011. J. Mater. Chem. 21, 16759–16782.
Zou, G.-Z., Liang, G.-D., Zhang, X.-L., 2011. Chem. Commun. 47, 10115–10117.